CrossMark

INDUSTRIAL APPLICATION

Surrogate based multidisciplinary design optimization of lithium-ion battery thermal management system in electric vehicles

Xiaobang Wang[1,2] · Mao Li[2,3] · Yuanzhi Liu[2] · Wei Sun[1] · Xueguan Song[1] · Jie Zhang[2]

Abstract A battery thermal management system (BTMS) is a complex system that uses various heat removal and temperature control strategies to keep battery packs at optimal thermal conditions, thereby improving the lifetime and safety of lithium-ion battery packs in electric vehicles (EVs). However, an optimal design of BTMS is still challenging, due to its large number of sub-systems and/or disciplines involved. To address this challenge, an air-based BTMS is hierarchically decoupled into four sub-systems and/or sub-disciplines in this paper, including the battery thermodynamics, fluid dynamics, structure, and lifetime model. A high-fidelity computational fluid dynamics (CFD) model is first developed to analyze the effects of key design variables (i.e., heat flux, mass flow rate, and passage spacing size) on the performance of BTMS. Aiming to perform the multidisciplinary design optimization (MDO) of BTMS based on the high-fidelity CFD model, surrogate models are developed using an automatic model selection method, the Concurrent Surrogate Model Selection (COSMOS). The surrogate models represent the BTMS performance metrics (i.e., the pressure difference between air inlet and outlet, the maximum temperature difference among battery cells, and the average temperature of the battery pack) as functions of key design parameters. The objectives are to maximize the battery lifetime and to minimize the battery volume, the fan's power, and the temperature difference among different cells. The MDO results show that the lifetime of the battery module is significantly improved by reducing the temperature difference and battery volume.

Keywords Battery thermal management system · Multidisciplinary design optimization · Concurrent surrogate model selection · System decomposition

1 Introduction

Currently, the lithium-ion battery is widely used in the electric vehicles (EVs), due to its advantages such as high voltage, high energy density, long cycle-life, no memory effect, and quick charging. However, there still exist a number of challenges in the design of lithium-ion battery and its associated systems in EVs, considering their multidisciplinary and system coupling characteristics. The battery usually experiences irregular jolts and large temperature variation, which makes its working conditions even harsher. In addition, the high heat generation and narrow space make the battery pack easily accumulate heat during the working process, which may cause volume expansion or even explosion of the battery. Due to the narrow range of the optimal operating temperature, the battery safety becomes one of the major concerns in EVs. Although the battery performance can be improved through structure optimization, the risks caused by the overcharge, over discharge, and excess temperature still cannot be fully avoided. Aiming to improve

✉ Jie Zhang
  jiezhang@utdallas.edu

1   Dalian University of Technology, Dalian 116024, China

2   The University of Texas at Dallas, Richardson,
    TX 75080, USA

3   Beijing Institute of Aerospace Testing Technology, Beijing,
    100074, China

the thermal performance of batteries, battery thermal management systems (BTMS) have been widely used in EVs, which utilize various heat removal and temperature control strategies to maintain the cells and battery packs at optimal thermal conditions (Ponchaut et al. 2014).

Different types of BTMS have been developed in the literature to enhance the battery performance, such as the air-based, liquid-based, phase change material-based, heat-pipe based, and hybrid systems. A review of some of these types of BTMS has been provided and discussed by Ling et al. (2014). Greco et al. (2014) developed a one-dimensional (1D) transient computational model of a prismatic lithium-ion battery with the heat pipe-based BTMS, which was tested and verified by an analytical model with time-dependent boundary conditions and a 3D numerical model. Huo et al. (2015) designed a mini-channel cold plate-based BTMS for a rectangular lithium-ion battery, based on which a 3D thermal model of the cooling system was established and simulated. It showed that the maximum temperature of the battery decreases with increasing the number of channels and inlet mass flow rate, and the cooling performance increases with increasing inlet mass flow rate. Somasundaram et al. (2012) proposed a 2D transient mathematical model to study a passive BTMS with and without phase change material (PCM) at various galvanostatic discharge rates.

The air-based BTMS has been widely applied in EVs due to its low cost, simple structure, and light weight. Choi and Kang (2014) modeled the thermal behavior of an air-based lithium-ion BTMS based on the battery's electrical and mechanical properties for determining the appropriate cooling capacity. Giuliano et al. (2012) developed an air-based BTMS employing metal-foam based heat exchanger plates, which was tested by an experiment using Altairnano 50 Ah cells. Fan et al. (2013) analyzed the 3D transient thermodynamics of an air-cooled BTMS using computational fluid dynamics (CFD), finding that the temperature uniformity could be improved by moderating the gap spacing size. Sun and Dixon (2014) developed a correlated 3D thermal model and an analytical design of experiments (DoE) approach to verify the "Z-type" flow battery pack with an air-based BTMS. It is found that the geometries of inlet and outlet significantly affected the lumped cell temperature, lumped cell temperature difference, and total pressure drop of the pack. Mohammadian et al. (2015) compared different strategies by inserting four different types of aluminum foam into the the flow channels of the air-cooled lithium-ion battery module, and found the desirable temperature uniformity and maximum temperature when two-third of the entire air flow channel was filled with aluminum metal foam.

To further improve the performance of BTMS, optimization methods have also been used in the BTMS designs. For example, Khan et al. (2014) proposed a techno-economic optimization model to investigate the feasibility of BTMS in different applications. Severino et al. (2014) used a Multi-Objective Particle Swarm Optimization (MOPSO) algorithm to optimize the BTMS design. Bahiraei et al. (2016) used a pseudo 3D coupled thermal-electrochemical model to optimize the weight of PCM required in the BTMS, considering the module size and battery cell spacing. The results showed that the use of PCM significantly reduced the battery temperature rise and kept a desirable temperature uniformity across the module. Hu et al. (2014) used support vector regression (SVR) with a double-loop search optimization process to estimate the state-of-charge (SOC) of the air-cooled battery pack in EVs. Ye et al. (2015) developed a numerical model to optimize the thermal performance of a heat pipe-based BTMS, and the BTMS performance was improved during fast charging. Padovani et al. (2013) optimized an energy management strategy for battery and BTMS in EVs using Pontryagin Minimum Principle. Javani et al. (2014b) optimized a newly-established PCM-based BTMS using the genetic algorithm (GA) to find the optimal exergy efficiency and total cost rate of the system. Park (2013) designed an air-based BTMS by conducting numerical calculations, and found that the required cooling performance by employing the tapered manifold and pressure relief ventilation without changing the layout/design of the existing battery system.

Though the mechanism and performance of BTMS have been well studied, most of the previous work only dealt with a single discipline or sub-system of the BTMS. However, the performance of battery is affected by a number of different components and disciplines involved in the battery system. For example, a typical air-based BTMS consists of an air supply system and battery cells. The battery cells supply the power to the vehicle motor as well as the air supply system, accompanied with heat generation. The air supply system provides the air to take away the heat and to cool the battery cells within the battery module. A better understanding of the interactions between different disciplines and/or sub-systems would help design and optimize the whole BTMS system. To this end, a multidisciplinary design optimization (MDO) framework of the BTMS is developed in this paper, with the aim of optimizing the design of different BTMS sub-systems simultaneously. The multidisciplinary modeling aims to help (i) understand the coupling effects among different disciplines and sub-systems, and (ii) formulate the system objectives and constraints for both the whole BTMS and sub-systems.

The remaining of the paper is organized as follows. Section 2 discusses the system analysis of an air-based BTMS and the overall MDO framework. Section 3 develops a high-fidelity CFD model and corresponding surrogate models to be used in the MDO of BTMS. Section 4 analyzes

the detailed configurations of four major disciplines/sub-systems, including the air supply system, battery thermo-dynamics, lifetime model, and structure. In Sections 5, the optimization results obtained by using the Multi-Disciplinary Feasible (MDF) method are obtained and discussed. Section 6 provides the concluding remarks and future work.
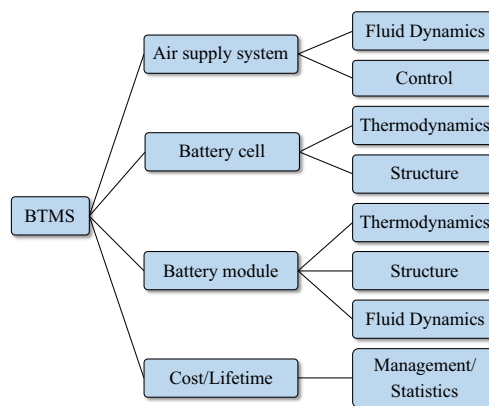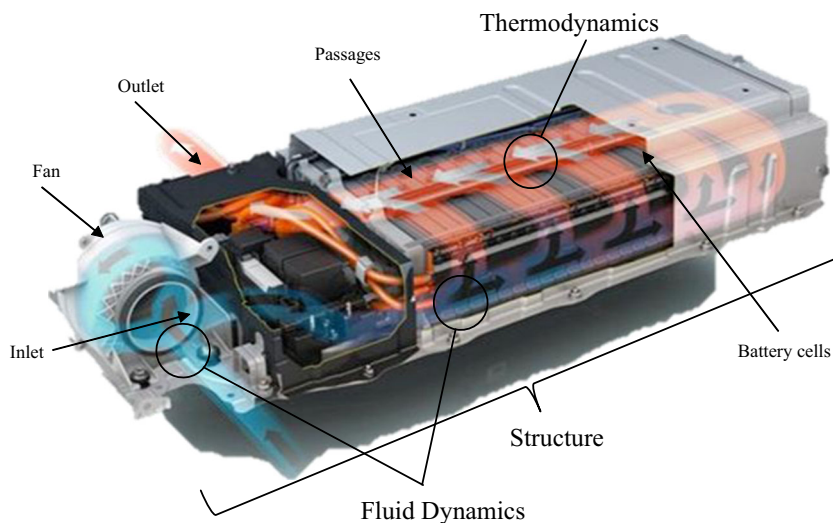
2 BTMS analysis

2.1 System decoupling of BTMS

As a highly integrated system, the major components of BTMS are densely assembled in a limited space. When the battery is working, every part of BTMS should work harmonically and steadily to maintain an efficient and safe running environment. So it is essential to first conduct a system analysis from a global view before performing the MDO study on BTMS. Figure 1 shows the physical system of an air-based BTMS, which contains a number of disciplines, such as the thermodynamics, fluid dynamics, and structure. By using a decomposition method of a hierarchical model, the BTMS can be decomposed into three main sub-systems, namely the air supply system, the battery cell, and the battery module, as shown in Fig. 2. Each sub-system can be further decomposed into secondary sub-systems that are categorized into different disciplines, e.g., the battery module can be categorized into the thermodynamics, fluid dynamics, and structure.

Besides the three major sub-systems, the battery lifetime/cost model should also be considered as a visional sub-system in the MDO of BTMS. This is because the battery lifetime/cost is an important performance index to assess the battery quality in the BTMS design or practical engineering.


Fig. 2 A hierarchical decomposition of BTMS

2.2 Extended design structure matrix (XDSM)

Due to the complexity of a MDO process, it is helpful to initially design a sketchy framework to illustrate the whole optimization process. For the BTMS design, a typical framework should include: (i) all the main sub-systems (or sub-disciplines), (ii) the coupling relationship of the design variables among different sub-disciplines, and (iii) the data flow between different sub-systems. The XDSM framework (Lambe and Martins 2012) is adopted in this paper to illustrate the MDO for BTMS. Figure 3 shows an sketchy XDSM framework of BTMS: (i) the boxes along the diagonal line represent the different sub-systems; (ii) the straight lines on the upper right of the diagonal line represent the flow direction of data input and output between different sub-systems; (iii) the boxes on the intersection points of the straight lines represent the design data being transmitted from an upstream sub-system to a downstream one; and (iv) the straight lines on the lower left of the diagonal line represent the data backflow, which contains the optimization

Fig. 1 A typical air-based BTMS scheme (GArtés 2012)
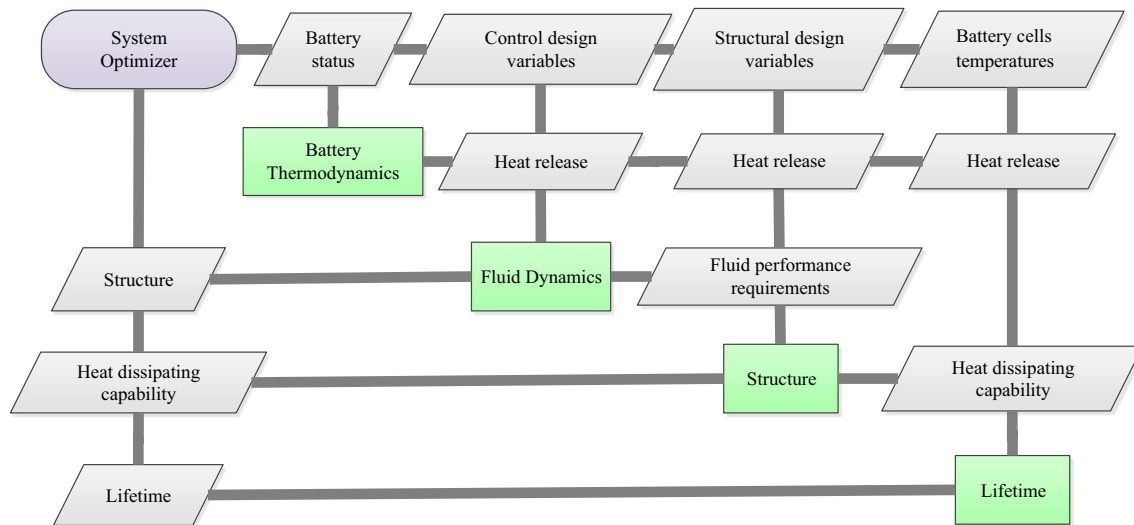
Fig. 3 XDSM framework for the MDO of BTMS

results of the sub-systems and relevant constraints. The running process starts from the upper right to the lower right, and then from the lower left to the upper left. The optimization process repeats until the design variables satisfy all the constraints.

It is observed from Fig. 3 that, the System Optimizer distributes the design variables and some important initial parameters into the corresponding sub-systems, such as the structural design variables being distributed into the sub-system of BTMS Structure, and the Battery Status parameters being distributed into the sub-system of Battery Thermodynamics. After the sub-systems complete their own disciplinary analysis, the sub-systems generate corresponding intermediate state variables and distribute these state variables downstream, such as the Battery Thermodynamics distributing the heat into the BTMS Structure, the Fluid Dynamics, and Lifetime. Then the sub-systems return the disciplinary objectives to the System Optimizer and complete a single circle. Importantly, a high-efficient parallel optimization strategy can be adopted to facilitate the whole optimization process.

Based on the sketchy MDO framework in Fig. 3, a targeted analysis of the corresponding disciplines can be conducted accordingly. The finally implemented framework could be appropriately modified based on the specific MDO algorithm/architecture. The final XDSM framework in the paper is provided in Section 5.

3 BTMS modeling

The BTMS is a complex engineering system that consists of a number of sub-models under different disciplines. For example, the layout of the battery cells affects the heat transfer; the air supply system consumes battery power besides

the cooling function. To successfully and effectively optimize the BTMS, a multidisciplinary design optimization (MDO) model of BTMS is developed.

A high-fidelity CFD model of an air-based BTMS is first developed to simulate the BTMS performance. This high-fidelity CFD model is accurate for simulation. However, it is challenging to perform the BTMS optimization directly based on the high-fidelity CFD model due to its expensive computational time. To this end, surrogate models are developed to represent the key BTMS performance metrics as functions of the design variables. The developed surrogate models are then integrated into the MDO architecture.

3.1 Air-based BTMS scheme

Figure 4 shows an air-based BTMS scheme with a lithium-ion battery module, which contains an air supply system and 36 lithium-ion prismatic cells. The dimension of a single cell is 65 mm × 151 mm × 16 mm. The battery cells are positioned vertically inside the module with evenly spaced cooling passages between neighboring cells. A cooling fan positioned on the side of the module is used to provide the cooling air to improve the thermal environment of the battery module. The cells are numbered 1 to 36 in sequence while the passages are numbered 1 to 37, with 1 denoting the cell or the passage closest to the fan. The air steam flows into the inlet manifold that is at the bottom of the battery module, and passes through the 37 passages. After cooling the battery cells, the air converges in the outlet manifold and flows out to the atmosphere. The height of the manifold is 20 mm. Note that, the inlet and outlet are on the same side of the battery module.

In the BTMS system, the fan is powered by the battery module. The ideal fan power (P_F) can be calculated by the
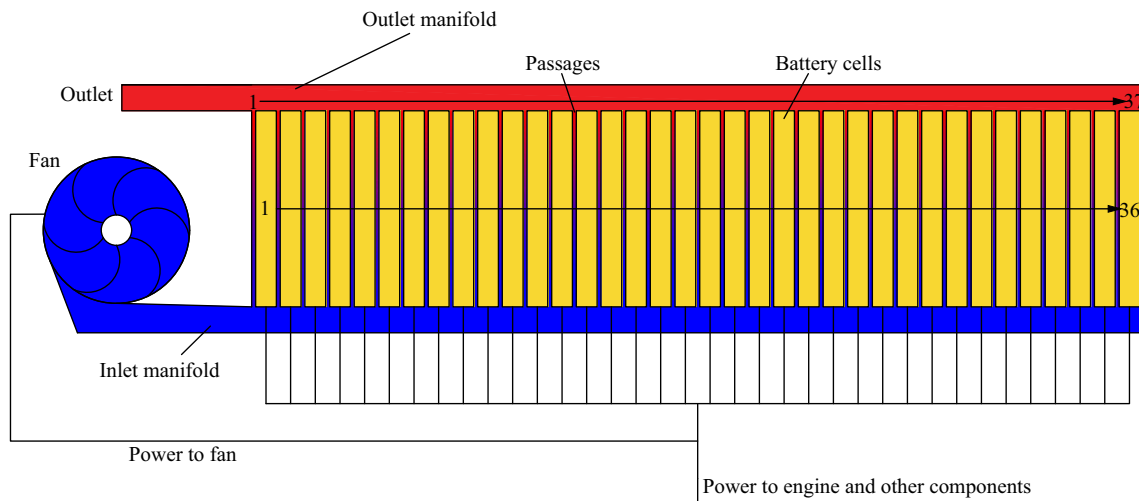
Fig. 4 A typical air-based BTMS scheme

volume flow rate ($\dot{V}$) and the pressure difference between the air inlet and outlet (Δp), which is described by (1).

$$P_F = \Delta p \dot{V} / \epsilon \qquad (1)$$

where ϵ is the efficiency of the fan. The equation shows that, for a given power value, high pressure air by the fan means a low volume flow rate. The heat generated by a battery cell can be calculated by (2).

$$q = I(U_o - U_c) = I^2 R_i \qquad (2)$$

where q is the heat generated by battery cell; I is the current flowing through the battery cell; U_o is the open circuit voltage; U_c is the cell voltage; and R_i is the direct current internal resistance of the battery cell. Equation (2) shows that if the power of the fan increases, the heat generated by the battery cell also increases. In this study, the heat is converted to the heat flux on the battery cell surface, as shown in (3).

$$\dot{q} = q / S \qquad (3)$$

where $\dot{q}$ is the heat flux; S is the heat exchange area between the air and battery cell. The heat is taken away by the cooling air. When the battery cell is at a heat balance, the heat can also be described by (4).

$$q = \rho \dot{V} c_p (T_{out} - T_{in}) \qquad (4)$$

where ρ is the density of air, and $\rho \dot{V}$ represents the mass flow rate of the air; c_p is a specific heat capacity; T_{out} and T_{in} are the air temperatures at the passage inlet and outlet, respectively. The heat exchange between the battery cell and the air is calculated by (5)

$$q = h(T_{cell} - T_{air}) \qquad (5)$$

where h is the heat transfer coefficient; T_{cell} is the battery cell temperature; T_{air} is the cooling air temperature. It is

seen from (4) and (5) that, the heat transfer significantly depends on the mass flow rate of the cooling air.

3.2 CFD model

In order to better optimize the performance of the battery in EVs with a high reliability, the temperature of the cooling air pumped into the BTMS by the fan is set to be 40 °C (e.g., a hot summer day). For the heat generated by battery cell, q (W), it is assumed that the heat only generates on the battery cell surface with a uniform heat flux, $\dot{q}$ (W/m^2). Based on the thermodynamics and fluid dynamics, three key parameters are selected as the inputs of surrogate models: the passage spacing size b (mm), the heat flux from the battery cell to the air, $\dot{q}$ (W/m^2), and the mass flow rate of the cooling air, $\dot{m}$ (kg/s). Three performance indexes are selected as the outputs, including the pressure drop, Δp (Pa), the maximum temperature difference, ΔT (°C), and average temperature, T_A (°C). Section 4 will further explain why these parameters and metrics are selected.

In this study, the commercial software ANSYS 17.0 is utilized. The realistic $\kappa - \varepsilon$ turbulence model and the SIMPLEC method are used to solve the simulations based on the steady and pressure-based solver. The second order upwind is used to disperse the pressure, density, and momentum equations. The thermal radiation transfer is assumed to be negligible in the work. The air inlet is specified as the mass flow rate boundary condition, whereas the outlet is set as the pressure outlet boundary condition. The surface of the battery cell is set as the heat flux condition. The adiabatic and no-slip wall boundary condition is applied to the walls of the battery module. Typical distributions of the total pressure and total temperature are shown in Fig. 5a and b, where $\dot{m} = 0.0281\ kg/s$, $\dot{q} = 204.38\ W/m^2$, and $b = 2.60\ mm$. It is observed that the mass flow rates in different passages are

(a) Total temperature
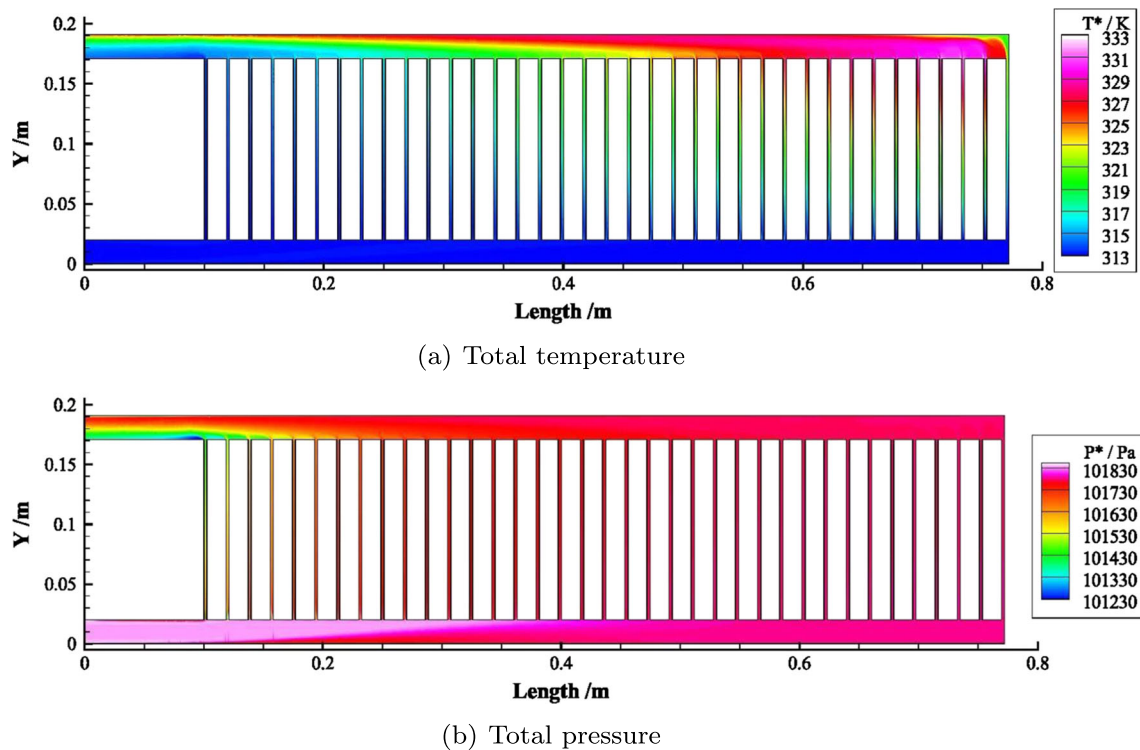
(b) Total pressure

Fig. 5 Distributions of the total pressure and the total temperature for a typical case

different, which results in the temperature difference among battery cells. Due to the different air temperatures at the passage inlet and outlet, the temperature distribution on the battery cell is uneven as well.
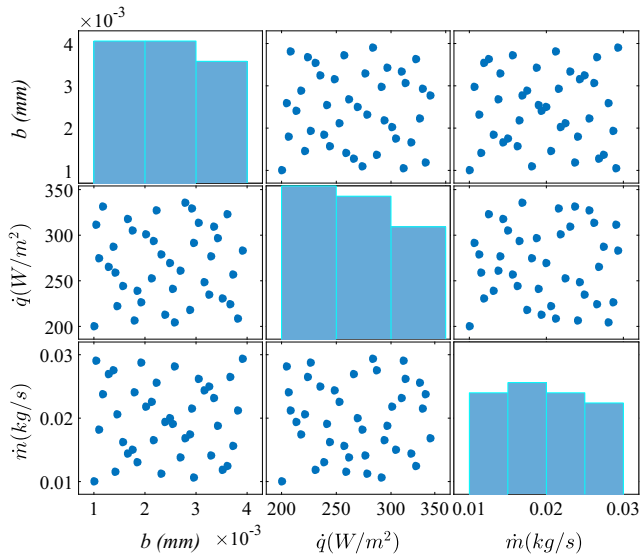
3.3 Surrogate models

When conducting a MDO for complex systems, one of the most significant challenges is how to successfully realize the data exchange and data fusion between the sub-system analysis modules and the system analysis module. In general, the sub-system analysis modules generate exchanging data between different disciplines through expensive simulations or experiments. To use these computationally expensive simulations or experiments in the MDO process, surrogate modeling provides a tractable and inexpensive approximation. Surrogate modeling consists of three major components: design of experiments (DoE), surrogate model construction, and accuracy evaluation. A variety of DoE sampling methods have been available in the literature, such as the Latin Hypercube Sampling (LHS) (McKay et al. 2000), Sobol sequence (Sobol' 1967), Orthogonal Array Design (OAD) (Rao 1947), Uniform Design (UD) (Fang et al. 2000), Full-factorial Design (FFD), and Central Composite Design (Box 1954). There also exist a number of methods for constructing surrogate models, such as the Response Surface Method (RSM), Kriging Model (Stein 2012), Radial Basis Function (RBF) (Buhmann 2003),

and Support Vector Regression (SVR) (Vapnik and Vapnik 1998).

The Sobol sequence is one of the most widely used DoE methods in surrogate modeling, which has been adopted in this study to generate 40 training points. Compared with other DoE methods, Sobol sequence provides a better uniformity, especially for high-dimensional problems (Zhang et al. 2013). The Sobol samples selection and distribution are shown in Fig. 6. The Concurrent Surrogate Model Selection (COSMOS) method proposed by Chowdhury et al. (2014) is adopted to select and construct the surrogate models.

3.4 Concurrent surrogate model selection (COSMOS) in the MDO of BMTS

As mentioned in Section 3.3, there are many model types that can be chosen to construct the surrogate model, some of which are listed in Table 1. Besides the model types, different types of kernel functions and hyper-parameters (as listed in Table 1) also significantly affect the accuracy of surrogate modeling. The combination of these three levels (model types, kernel functions, and hyper-parameters) can produce a variety of characteristically different surrogate models. For example, 4 kinds of kernel functions for the Kriging model are listed in Table 1. Each kernel function has its own hyper-parameters. More importantly, when using surrogate models during the MDO process, engineers/users

Fig. 6 Distribution of the DoE samples in the MDO of BTMS

criterion and find the best configuration for surrogate modeling concurrently and automatically. The PEMF, a robust implementation of sequential k-fold cross-validation, establishes intermediate surrogates at each iteration and predicts the error distributions by using the estimated median and the maximum errors. Then the estimated modes of the error distributions are used to predict the expected median and maximum errors in the final surrogate model. In the COSMOS framework, there are five different error criterions predicted by PEMF serving as the candidates for selection, such as the modal values and the variance values of the median/maximum errors. In this study, the modal values of the median and the maximum errors in the surrogate model are used as the two selection criteria to conduct the automatic selection for surrogate models. The Cascaded technique and the One-Step technique are two major approaches to implement COSMOS (Chowdhury et al. 2014). In the One-Step technique, the global pool of model-kernel candidates is divided into three smaller pools of model-kernel candidates (ϕ_n, $n = 1, 2, 3$) based on the number of constituent hyper-parameters (n) involved (Chowdhury et al. 2014). By using the PEMF as error predication, the optimization seeks to minimize the surrogate model error. Then the optimal configuration selection can be performed separately (in parallel) for each candidate pool. After obtaining the Pareto optimal configurations of each pool, the Pareto optimal configurations of all the global pool can be obtained by a Pareto filter. Finally, the optimal configuration of the surrogate model can be selected in accordance with specific conditions of the optimization problem. In this paper, the PEMF toolbox is adopted to establish the COSMOS framework (Mehmani et al. 2015). The One-Step technique using the Non-Dominated Sorting Genetic Algorithm II (NSGA-II) (Deb et al. 2002) is implemented in the COSMOS framework to perform the optimization, and both

usually cannot fully master all the disciplines and perfectly configure each discipline with a suitable surrogate model. So the selection of surrogate model types and configurations for any given training data is often far from intuitive (Chowdhury et al. 2014), and an effective model selection approach is desired to address this challenge.

In this paper, the COSMOS method proposed by Chowdhury et al. (2014) is adopted to automatically determine the specific configurations (such as optimal model type, kernel function, and hyper-parameters) of surrogate models for MDO. This approach can achieve a reasonable allocation at all the three levels from a pool of diverse model candidates, including the RBF, Kriging, SVR, etc.. The COSMOS uses the Predictive Estimation of Model Fidelity (PEMF) (Mehmani et al. 2015) to evaluate the

Table 1 The configurations of surrogate models

Model type	Kernel function	Expression	Hyper-Parameter
RBF	Linear	r	None
	Cubic	r^3	None
	Gaussian	$e^{-r^2/2\sigma}$	Shape parameter (σ)
	Multiquadric	$(r^2 + \sigma^2)^{0.5}$	Shape parameter (σ)
Kriging	Linear	$\max(1 - \theta r, 1)$	Correlation parameter (θ)
	Exponential	$e^{-\theta r}$	Correlation parameter (θ)
	Gaussian	$e^{(-\theta r)^2}$	Correlation parameter (θ)
	Spherical	$1 - 3\xi^2 + 2\xi^3$	Correlation parameter (θ)
		$\xi = \max(1 - \theta r, 1)$	
SVR	Linear	(x_i^T, x_j)	Penalty parameter (C)
	Gaussian	$e^{-\gamma\|x_i - x_j\|}, \gamma > 0$	Penalty parameter (C)
			Kernel parameter (γ)
	Sigmoid	$\tanh(\gamma x_i^T x_j + r)$	Penalty parameter (C)
			Kernel parameter (γ)

the sample size and the generation number are set to be 100.

4 Configurations of BTMS sub-systems

4.1 Battery thermodynamics

During charge and discharge, lithium-ion cells generate a mass of heat from various chemical and electrochemical reactions. All the generated heat is assumed to be spatially uniform and attributed to the internal Ohmic resistance (Javani et al. 2014a). The accumulation of generated heat can increase the battery temperature; the uneven distribution of the generated heat can lead to an uneven temperature distribution in the battery pack among different cells and modules. Thus, two main problems can be triggered (Rao and Wang 2011): i) the high temperature during charge and discharge may make the battery temperature exceed permissible levels and decrease the battery performance. ii) the uneven temperature distribution in the battery pack may lead to a localized deterioration. In order to obtain a better vehicle performance, reliability, and safety, the battery average temperature T_A (°C) and the maximum temperature difference ΔT (°C) among different cells are chosen to be the two performance metrics of the thermodynamics in the air-based BTMS.

In this paper, two surrogate models are established to represent the performance metrics of the thermodynamics as functions of design parameters. As mentioned in Section 3.4, the COSMOS is used to select the most appropriate surrogate models. By using the NSGA-II, the final Pareto optimal solutions of T_A and ΔT marked by red circles are shown in Fig. 7a and b, respectively, where ϕ_i denotes the ith hyper-parameter class classified based on the number of hyper-parameters. By considering both of the maximum error and median error, the selected best

configuration of the surrogate model of the average battery temperature T_A is: the RBF model with a Multiquadric basis function and a shape parameter, $\sigma=0.2819$. The median error and maximum error of the established RBF of T_A are 0.0184 and 0.0236, respectively. For the surrogate model of the maximum temperature difference ΔT, the RBF model with a Cubic basis function is selected, and the median error and maximum error are 0.0114 and 0.0439, respectively. Figure 8a and b show the approximated models of T_A and ΔT, and the surrogate models are denoted by (6) and (7).

$$T_A = f_s(\dot{m}, \dot{q}, b) \tag{6}$$

$$\Delta T = f_s(\dot{m}, \dot{q}, b) \tag{7}$$

4.2 Fluid dynamics (air)

In the air-based BTMS, the cooling air is pumped by a fan, flowing through the passages between different cells and flowing out of the battery module through the outlet, as shown in Fig. 4. There is pressure drop occuring due to the frictional resistance in the pipes/ducts, the expansion and contraction losses at the and the outlet of the module (Park and Jung 2013). The pressure drop has a great effect on the required pump size, which influences the energy consumption and vehicle integration by requiring mechanically stronger cooling plates to withstand the higher pressure forces, leading to higher costs (Smith et al. 2014). So the pressure drop Δp (Pa) is taken as a performance metric of the fluid dynamics for the air-based BTMS.

The surrogate model of the pressure drop Δp is built to represent the performance metric of the fluid dynamics as a function of design parameters. By adopting the COSMOS method, the final Pareto optimal solutions marked by red circles are shown in Fig. 9, where ϕ_i denotes the

(a) Surrogate model selection of T_A

(b) Surrogate model selection of ΔT
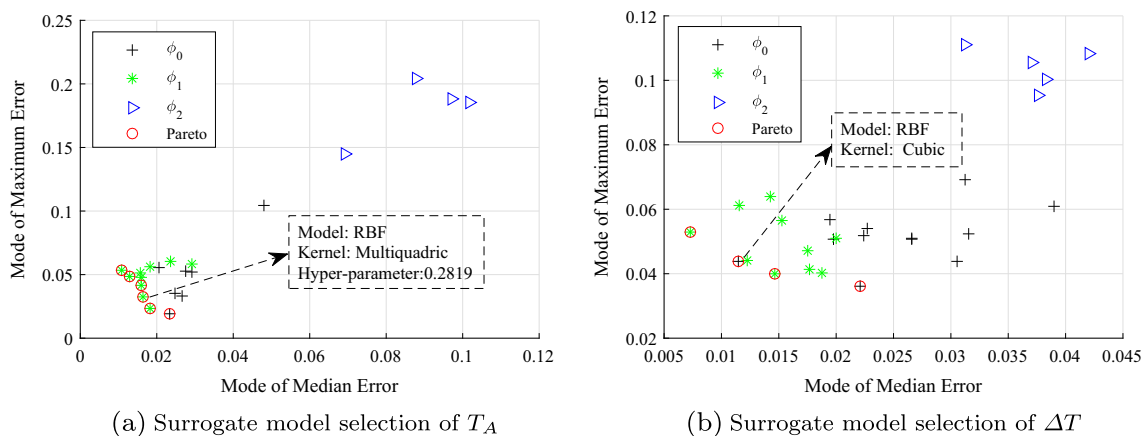
Fig. 7 Surrogate models selection of T_A and ΔT

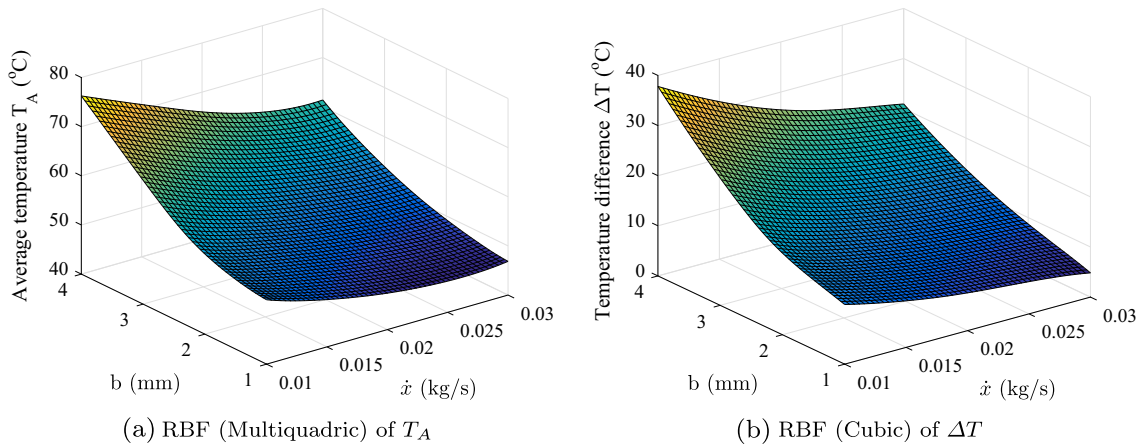(a) RBF (Multiquadric) of T_A

(b) RBF (Cubic) of ΔT

Fig. 8 Surrogate models of T_A and ΔT

ith hyper-parameter class classified based on the number of hyper-parameters. By considering both of the maximum error and median error, the selected best configuration of the surrogate model of the pressure drop (Δp) is: the RBF model with a Multiquadric basis function and a shape parameter, $\sigma = 0.2776$. The median error and maximum error of the RBF model the pressure drop Δp are 0.0207 and 0.0503, respectively. Figure 10 shows the surrogate model of Δp.

$$\Delta p = f_s(\dot{m}, \dot{q}, b) \tag{8}$$

4.3 Lifetime model analysis

The semi-empirical lifetime model of the lithium-ion battery proposed by Wang et al. (2014) is adopted in this paper. This lifetime model is obtained through a well-designed experiment by using three important correlation parameters collected from a large cycle-test matrix, i.e., the time, the temperature, and the discharge rate (Wang et al. 2016). As defined by Wang et al. (2014), this lifetime model takes both

the calendar loss and capacity loss into account, described as follows:

$$Q_{loss} = Q_{loss}^{Calendar} + Q_{loss}^{Cycle} \tag{9}$$

$$Q_{loss}^{Calendar} = f e^{-E_a/R(T+273)} t^{0.5} \tag{10}$$

$$Q_{loss}^{Cycle} = B_1 \cdot e^{B_2 \cdot I_{rate}} A_h \tag{11}$$

$$B_1 = a(T+273)^2 + b(T+273) + c \tag{12}$$

$$B_2 = d(T+273) + c \tag{13}$$

Where $Q_{loss}^{Calendar}$ denotes the calendar loss (%); Q_{loss}^{Cycle} denotes the capacity loss (%); t denotes the time (day); T denotes the battery temperature (°C); I_{rate} denotes the charge/discharge rate expressed as a C-$rate$; B_1 denotes the pre-exponential factor; B_2 denotes the exponential factor; A_h denotes the Ah-throughput (Ah) that is function of time t. The remaining relevant parameters are explained in Table 2 and all the values are specific to the lithium-ion battery.
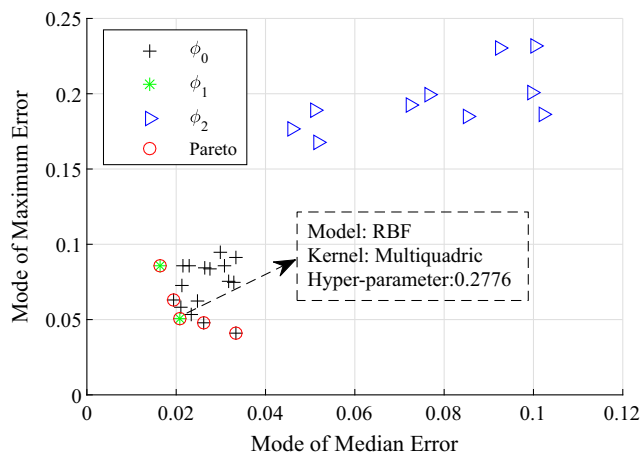

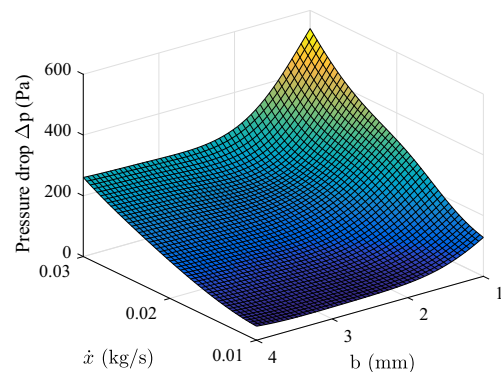**Fig. 9** Surrogate model selection of Δ_p

Fig. 10 RBF (Multiquadric) of Δp

Table 2 The parameters used in the lifetime model of the lithium ion battery (Wang et al. 2014)

Parameter (unit)	Meaning	Value
E_a (J/mol)	Activation energy	2.45×10^4
R $(J/(mol \cdot K)$	Gas constant	8.314
a $(Ah^{-1}K^{-2})$	Coefficient	8.61×10^{-6}
b $(Ah^{-1}K^{-1})$	Coefficient	-5.13×10^{-3}
c (Ah^{-1})	Coefficient	0.763
d $(1/K-(C-rate))$	Coefficient	-6.7×10^{-3}
e $(C-rate^{-1})$	Coefficient	2.35
f $(day^{-0.5})$	Pre-exponential factor	14,876

By assuming that the EV is driven two hours per day (e.g., 1-hour driving distance between home and workplace), the EV should be charged once every four days. The *C-rate* is set to be 3.5 *C* in this paper. Then the relationship between the battery lifetime and key battery design parameters can be explored. Usually, the battery lifetime is defined as the period from the initial starting time to the time when the battery loses 20-30% of its original storage capacity (Wang et al. 2016). In this paper, the critical capacity loss of lithium-ion battery is set to be 30%. The effects of the battery used time and battery temperature on the battery capacity loss are shown in Fig. 11. In Fig. 11a, the red semitransparent plane is the critical level of 30% battery capacity loss and the red intersection curve denotes the critical line of the battery life. Only the points on the response surface below the semitransparent critical plane mean the battery is working within the span of lifetime. It is observed that the battery capacity loss increases with the increasing used time and battery temperature. More significantly, the capacity loss rate of the lithium-ion battery rises more drastically with the increasing battery temperature. Figure 11b shows the battery lifetime affected by

the battery temperature in the range of 40 °C to 65 °C in more detail. It is observed from Fig. 11b that, if the battery temperature works at 40 °C, the battery lifetime is more than ten years. With the increasing battery temperature, the battery life experiences a quick decrease with a diminishing acceleration corresponding to equal temperature decrease. So, if the battery temperature is reduced by even a small amplitude in the sensitive range approximately from 40 °C to 55 °C, the battery lifetime will have a significant rise. Thus, this paper aims to reduce the battery's working temperature by improving the performance of BTMS.

4.4 Structure analysis

The battery miniaturization (with high energy density) has become a trend in the EV industry. By realizing the miniaturization, the inner space of the EV can be saved and the restrictions of the automotive chassis and suspension system will be reduced. In this paper, the battery volume is also taken into account in the MDO process. The battery volume can be divided into two parts, including the volume of the battery module (V_c) and the volume of the fan (V_F). The volume of the battery module (V_c) can be estimated by the volume of a cuboid abstracted from the battery module. Generally, the fan's volume increases with the increasing fan power. Thus the fan's volume can be described as a function of the fan's output power. The volume of the battery can be described as follows:
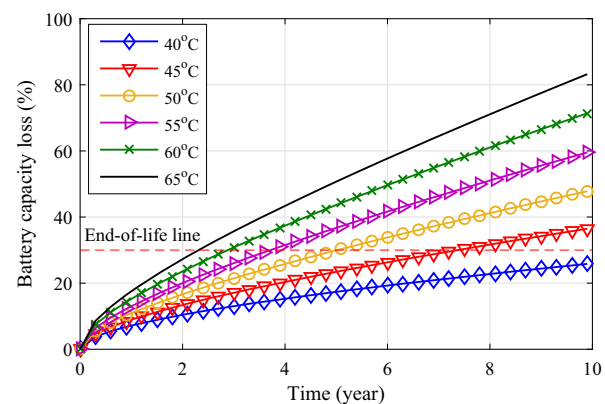
$$V = V_c + V_F \tag{14}$$

$$V_c = w_c \cdot h_c \cdot l_c \tag{15}$$

$$V_F = \kappa \cdot P_F \tag{16}$$

Where, w_c, h_c, and l_c are the width, the height, and the length of the battery module, respectively; κ is the
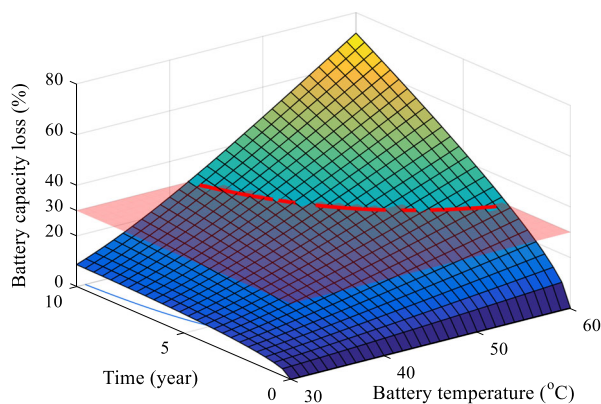
(a) The relationship among battery used time, temperature, and capacity loss

(b) The battery capacity loss affected by different battery temperatures

Fig. 11 The battery capacity loss caused by the battery used time and battery temperature

proportionality coefficient, and $\kappa = 5 \times 10^{-5} m^3/W$ in this paper.

5 MDO of BTMS

5.1 MDO establishment

As mentioned in Section 3.2, the temperature of the cooling air pumped into the BTMS is set to be 40 °C to ensure the reliability of the MDO in this paper. According to the BTMS disciplinary analysis in Section 4, three design variables are selected as shown in (17), including the mass flow rate $\dot{m}$ (kg/s), the heat flux $\dot{q}$ (W/m^2), and the passage spacing size b (mm).

$$\mathbf{X} = [\dot{m}, \dot{q}, b] \tag{17}$$

Based on the physical characteristics and performance requirement of the lithium-ion battery used in EVs, the upper and lower bounds of the three design variables are defined in Table 3.

There are four objectives in the BTMS optimization: (i) the battery lifetime t ($year$) is maximized; (ii) the maximum temperature difference ΔT (°C) among battery cells is minimized; (iii) the power consumed by fan P_F (W) is restrained within a reasonable range so as to save more power for the EV running and to minimize the size of the fan; (iv) the volume of the battery V (m^3) is minimized. This multi-objective optimization problem can be transformed into a single-objective optimization problem by distributing different weights to each objective. So the final objective function is described as:

$$f = \left(\frac{1}{t}\right)^{\lambda_1} \Delta T^{\lambda_2} \cdot P_F^{\lambda_3} \cdot V^{\lambda_4} \tag{18}$$

where λ_i's are the weights. In this paper, large weights are assigned to the battery lifetime and battery temperature difference, $\lambda_1 = 0.6$, $\lambda_2 = 0.2$, $\lambda_3 = 0.1$, and $\lambda_4 = 0.1$.

The objectives and constraints can mutually transform between each other in the MDO process; optimization objectives in one sub-system may be used as constraints in another sub-system (Sun et al. 2016). According to the requirement of the physical structure and performance associated with different disciplines, including the fluid

Table 3 Upper and lower bounds of design variables

Design parameter (unit)	Lower bound	Upper bound
$\dot{m}$ (kg/s)	0.01	0.03
$\dot{q}$ (W/m^2)	200.00	340.00
b (mm)	1.00	4.00

dynamics, thermodynamics, and structure, the constraints in this study are summarized in (19):

$$\begin{cases} g_1 = P_F - 4 \\ g_2 = -\Delta p + 100 \\ g_3 = \Delta p - 300 \\ g_4 = T_A - 50 \\ g_5 = V - 0.012 \\ g_6 = \dot{q} - 300 \end{cases} \tag{19}$$

It should also be noted that the battery simultaneously provides power for both the cooling fan and the vehicle. So the heat generation of all the battery cells can be divided into two parts, as illustrated in (20):

$$\dot{q} = \xi \frac{\Delta p \dot{m}}{36 A \rho \eta} + \dot{q}_v \tag{20}$$

where ξ is the coefficient of heat production; η is the scale coefficient of the heat generation of the fan; A (m^2) is the surface area of the battery cell; ρ (kg/m^3) is the air density; $\dot{q}_v$ (W/m^2) is the heat generation due to vehicle operations or battery charging.

The overall MDO model of the BTMS is formulated as:

$$\begin{cases} \text{find } \mathbf{X} \\ \min f = (\frac{1}{t})^{\lambda_1} \Delta T^{\lambda_2} \cdot P_F^{\lambda_3} \cdot V^{\lambda_4} \\ \text{s.t. } g_i \leq 0 (i = 1, 2, 3, 4, 5, 6) \\ \Delta p = f(\dot{m}, \dot{q}, b) \\ \dot{q} = \xi \frac{\Delta p \dot{m}}{36 A \rho \eta} + \dot{q}_v \end{cases} \tag{21}$$

5.2 MDO architecture

To overcome the computational challenge and find efficient optimization algorithms, a number of MDO architectures have been proposed in the literature (Perez et al. 2004). MDO architectures can be divided into two main categories: single-level formulations (e.g., All-At-Once (AAO)) (McAllister et al. 2005), Multi-Disciplinary Feasible (MDF)
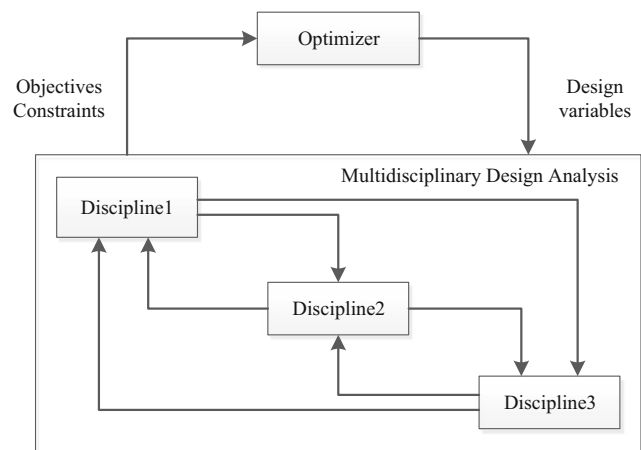

Fig. 12 A typical Multi-Disciplinary Feasible (MDF) architecture

(Cramer et al. 1994), Individual Discipline Feasible (IDF) (Dennis and Lewis 1994) and multi-level formulations (e.g., Collaborative Optimization (CO) (Gage and lan Sobieski 1996), Concurrent Subspace Optimization (CSSO) (Sellar et al. 1996), and Bi-Level Integrated Synthesis System (BLISS) (Sobieszczanski-Sobieski et al. 2000)). By considering the state variables, objective functions, constraints, and the number of design variables, the MDF architecture is chosen to conduct the MDO of BTMS in this paper. As shown in Fig. 12, the system optimizer distributes the design variables into the multiple disciplinary analysis (MDA) module that is an indispensable analyzer to realize the interdisciplinary consistency. In the MDA module, each individual discipline receives the system design variables from the system optimizer and the coupled design variables from other disciplines. The MDA analyzer transfers the state variables to the system optimizer to evaluate the constraints and objectives.

The XDSM, a new diagram for visualizing the MDO process is built to explain the MDF architecture of the BTMS optimization, as illustrated in Fig. 13. The parameters x_i's are the three design variables and y_i's are the two coupling state variables in the MDF process. In this paper, the BTMS is decoupled into four sub-disciplines, namely the battery thermodynamics, the fluid dynamics (air), the structure, and the battery lifetime. Each of the sub-discipline has its own model however with different parameters coupled with each other. As shown in Fig. 13, the parameter coupling analysis between different disciplines needs to be performed first by the MDA module.

Then the MDF process sequentially runs from Step 1 to Step 7. After iterative computations, the optimal results can be obtained.

5.3 MDO results

The initial values of mass flow rate (m_0) and passage spacing size (b_0) are set as 0.02 kg/s and 3.00 mm, respectively. The parameter of $\dot{q}_0$ is a state design variable coupled with the pressure drop Δp, which can be obtained in every iteration during the MDO process. The initial pressure drop Δp and heat flux $\dot{q}_0$ are set as 180.00 Pa and 260.00 W/m^2, respectively, and $\dot{q}_v$ is set to be 250.00 W/m^2. The optimization histories of the objectives are shown in Fig. 14, where the convergence curves approach to the optimal solutions at the 67th iteration after some remarkable fluctuations, with the objective value of 0.49. As illustrated from Fig. 14b-e, the optimal temperature difference ΔT is 20.50 °C, the optimal volume of the battery is 0.0099 m^3, the optimal fan power is 3.36 W, and the optimal lifetime of the lithium-ion battery is 5.16 $year$.

Table 4 shows the performance improvement of the BTMS after the optimization. For the design variables, the mass flow rate $\dot{m}$ decreases from 0.0200 kg/s to 0.0182 kg/s by 9.00 %, the heat flux $\dot{q}$ increases from 251.08 W/m^2 to 251.17 W/m^2 by 0.04 %, and the passage spacing size b decreases from 3.00 mm to 1.70 mm by 43.33 %. For the constraints, the average temperature is reduced from 55.44 °C to 49.56 °C by 10.58 %, and the pressure drop Δp is increased from 120.08 Pa to 142.90 Pa by 19.01%. For
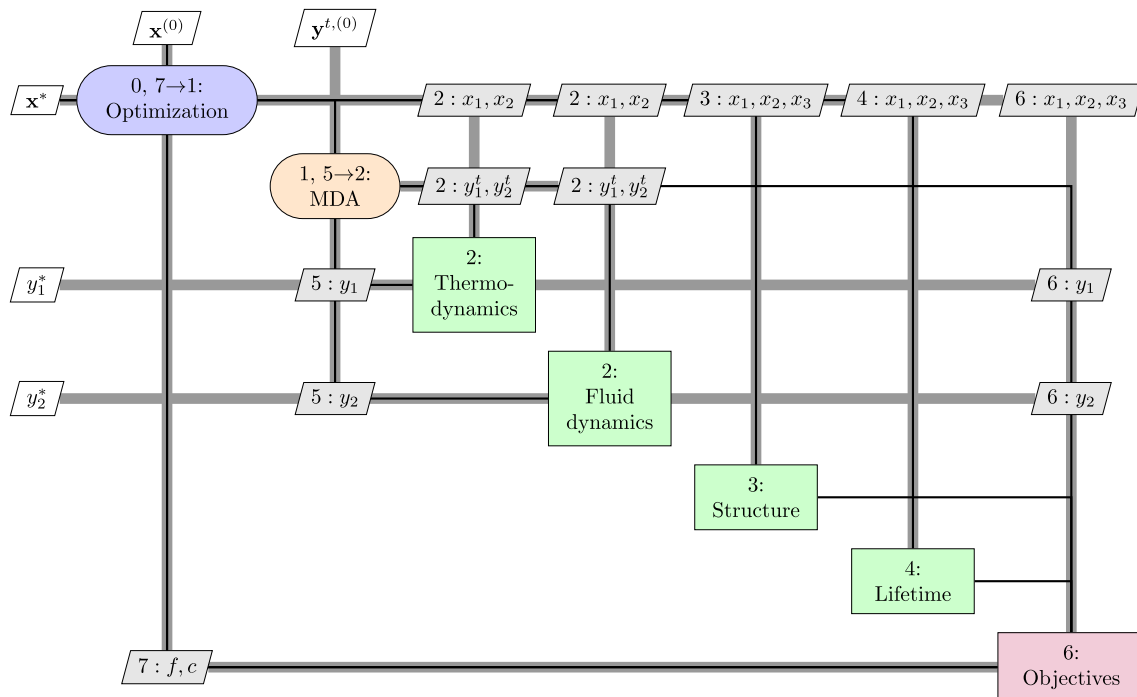

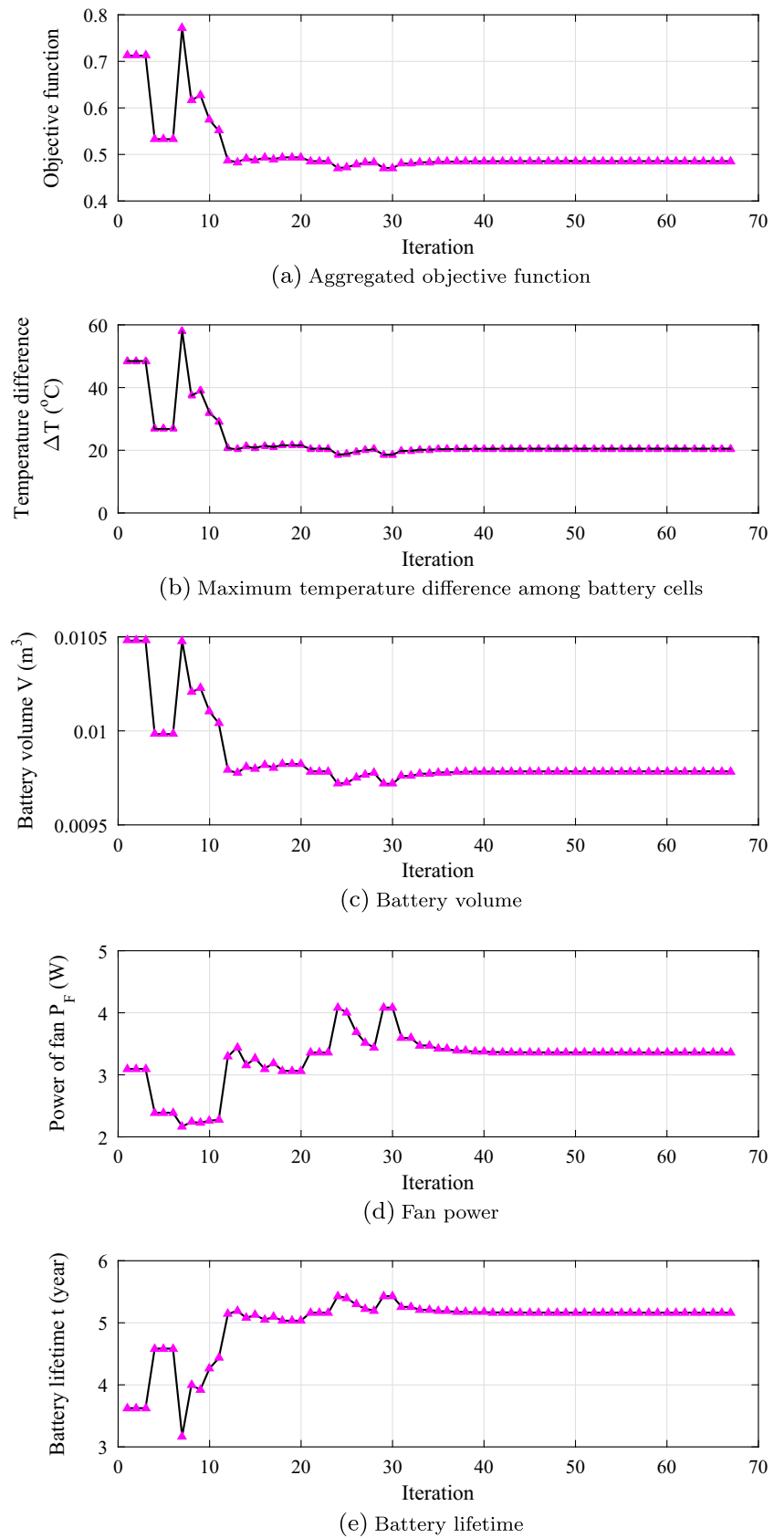**Fig. 13** XDSM framework of MDF for the BTMS

Fig. 14 The optimization history of MDO using MDF

(a) Aggregated objective function

(b) Maximum temperature difference among battery cells

(c) Battery volume

(d) Fan power

(e) Battery lifetime

Table 4 BTMS optimization results

	Parameter	Initial value	Range	Optimal value	Improvement
Design variables	$\dot{m}\ (kg/s)$	2.00×10^{-2}	[0.01, 0.03]	1.82×10^{-2}	-9.00%
	$\dot{q}\ (W/m^2)$	251.08	[100.00, 340.00]	251.17	$+0.04\%$
	b (mm)	3.00	[1.00, 4.00]	1.70	-43.33%
Constraints	T_A (°C)	55.44	[0, 50.00]	49.56	-10.58%
	$\Delta p\ (Pa)$	120.08	[0, 320.00]	142.90	$+19.01\%$
Objectives	P_F (W)	3.10	min	3.36	$+8.48\%$
	ΔT (°C)	48.45	min	20.50	-57.70%
	$V\ (m^3)$	1.05×10^{-2}	min	0.98×10^{-2}	-6.67%
	$t\ (year)$	3.62	min	5.16	$+42.37\%$

Note: the "+" sign means increase, and the "-" sign means decrease.

the objectives, the temperature difference decreases significantly by 57.70 % from 48.45 °C to 20.50 °C. According to the surrogate models of T_A and ΔT in Fig. 8, the decrease of the passage spacing size b and the mass flow rate $\dot{m}$ enables the reduction of the battery average temperature and temperature difference. The power consumed by the fan is increased from 3.10 W to 3.36 W by 8.48 %. This increase of fan power is mainly because of the increase of the pressure drop Δp from 120.08 Pa to 142.90 Pa, to better cool the battery temperature down. Also the volume of battery is reduced by 6.67 % from 0.0105 m^3 to 0.0098 m^3. Finally, the optimal lifetime of the lithium-ion battery is 5.16 year compared to the initial value of 3.62 year. As discussed in Section 4.3, the battery temperature has a direct effect on the battery lifetime. Figure 15 shows the relationship between the battery lifetime and the battery temperature during the optimization iteration. It shows that the decrease of the battery temperature from the 1st iteration to 67th

iteration drives the battery lifetime to increase significantly by 42.37 %.

6 Conclusion

A surrogate-based multidisciplinary design optimization (MDO) of the air-based battery thermal management system (BTMS) was developed in this paper. By using a decomposition method of a hierarchical model, the BTMS was decoupled into four disciplines, including the fluid dynamics, the thermodynamics, the structure, and the battery lifetime. The corresponding disciplinary analysis was conducted as well. To perform the MDO based on the high-fidelity CFD models, three surrogate models, selected automatically by Concurrent Surrogate Model Selection (COSMOS) method, were built to represent the corresponding sub-system performance metrics. Design parameters of the mass flow rate, heat flux, and passage spacing size were optimized by a MDF architecture, and the MDO objectives were to maximize the battery lifetime and minimize the battery cells temperature difference, fan power, and battery volume. The optimization results showed that the lifetime of the battery module was significantly improved by reducing the temperature difference and battery volume.

In this paper, the lithium-ion battery pack with the air-based BTMS is assumed to have the same battery spacing size. However, different spacing sizes could be used at different passages to improve the thermal performance, which could be a significant extension for the battery optimization in the future work. Besides, the sizes of the inlet, outlet, and the passageway could also be taken into account in the MDO.
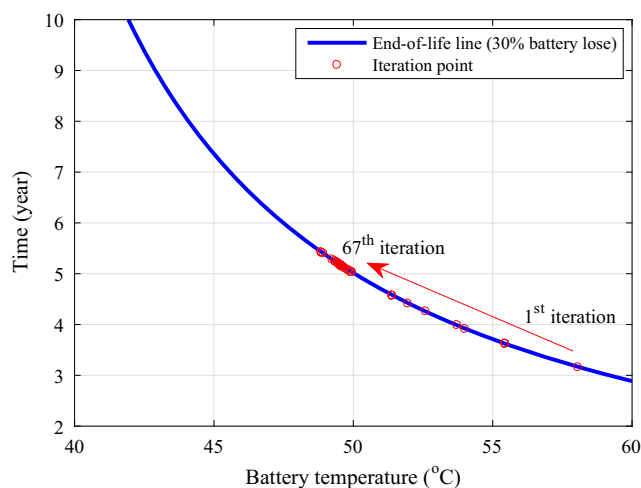
Fig. 15 The iteration history of the lifetime related to the battery temperature

References

Bahiraei F, Fartaj A, Nazri GA (2016) Numerical investigation of active and passive cooling systems of a lithium-ion battery module for electric vehicles. Tech. rep., SAE Technical Paper

Box GE (1954) The exploration and exploitation of response surfaces: some general considerations and examples. Biometrics 10(1):16–60

Buhmann MD (2003) Radial basis functions: theory and implementations. Camb Monogr Appl Comput Math 12:147–165

Choi YS, Kang DM (2014) Prediction of thermal behaviors of an air-cooled lithium-ion battery system for hybrid electric vehicles. J Power Sources 270:273–280

Chowdhury S, Mehmani A, Messac A (2014) Concurrent surrogate model selection (cosmos) based on predictive estimation of model fidelity. In: ASME 2014 International Design Engineering Technical Conferences and Computers and Information in Engineering Conference. American Society of Mechanical Engineers, pp V02BT03A026–V02BT03A026

Cramer EJ, Dennis JJr, Frank PD, Lewis RM, Shubin GR (1994) Problem formulation for multidisciplinary optimization. SIAM J Optim 4(4):754–776

Deb K, Pratap A, Agarwal S, Meyarivan T (2002) A fast and elitist multiobjective genetic algorithm: Nsga-ii. IEEE Trans Evol Comput 6(2):182–197

Dennis J, Lewis RM (1994) Problem formulations and other optimization issues in multidisciplinary optimization, Colordao, vol, Colorado Springs

Fan L, Khodadadi J, Pesaran A (2013) A parametric study on thermal management of an air-cooled lithium-ion battery module for plug-in hybrid electric vehicles. J Power Sources 238:301–312

Fang KT, Lin DK, Winker P, Zhang Y (2000) Uniform design: theory and application. Technometrics 42(3):237–248

Gage RBP, Ian Sobieski IK (1996) Implementation and performance issues in collaborative optimization

GArtés D (2012) Baterías de coches eléctricos e híbridos, hoy [estado de la tecnología del automóvil]. Website. http://www.diario-motor.com/tecmovia/2012/03/14/baterias-de-coches-electricos-e-hibridos-hoy-estado-de-la-tecnologia-del-automovil

Giuliano MR, Prasad AK, Advani SG (2012) Experimental study of an air-cooled thermal management system for high capacity lithium–titanate batteries. J Power Sources 216:345–352

Greco A, Cao D, Jiang X, Yang H (2014) A theoretical and computational study of lithium-ion battery thermal management for electric vehicles using heat pipes. J Power Sources 257:344–355

Hu J, Hu J, Lin H, Li X, Jiang C, Qiu X, Li W (2014) State-of-charge estimation for battery management system using optimized support vector machine for regression. J Power Sources 269:682–693

Huo Y, Rao Z, Liu X, Zhao J (2015) Investigation of power battery thermal management by using mini-channel cold plate. Energy Convers Manag 89:387–395

Javani N, Dincer I, Naterer G, Rohrauer G (2014a) Modeling of passive thermal management for electric vehicle battery packs with pcm between cells. Appl Therm Eng 73(1):307–316

Javani N, Dincer I, Naterer G, Yilbas B (2014b) Exergy analysis and optimization of a thermal management system with phase change material for hybrid electric vehicles. Appl Therm Eng 64(1):471–482

Khan MR, Nielsen MP, Kær SK (2014) Feasibility study and techno-economic optimization model for battery thermal management system. In: Proceedings of the 55th conference on simulation and modelling (SIMS 55), modelling, simulation and optimization, 21-22 october 2014, vol 108. Linköping University Electronic Press, Aalborg, pp 16-27

Lambe AB, Martins JR (2012) Extensions to the design structure matrix for the description of multidisciplinary design, analysis, and optimization processes. Struct Multidiscip Optim 46(2):273–284

Ling Z, Zhang Z, Shi G, Fang X, Wang L, Gao X, Fang Y, Xu T, Wang S, Liu X (2014) Review on thermal management systems using phase change materials for electronic components, li-ion batteries and photovoltaic modules. Renew Sust Energ Rev 31:427–438

McAllister CD, Simpson TW, Hacker K, Lewis K, Messac A (2005) Integrating linear physical programming within collaborative optimization for multiobjective multidisciplinary design optimization. Struct Multidiscip Optim 29(3):178–189

McKay MD, Beckman RJ, Conover WJ (2000) A comparison of three methods for selecting values of input variables in the analysis of output from a computer code. Technometrics 42(1):55–61

Mehmani A, Chowdhury S, Messac A (2015) Predictive quantification of surrogate model fidelity based on modal variations with sample density. Struct Multidiscip Optim 52(2):353–373

Mohammadian SK, Rassoulinejad-Mousavi SM, Zhang Y (2015) Thermal management improvement of an air-cooled high-power lithium-ion battery by embedding metal foam. J Power Sources 296:305–313

Padovani TM, Debert M, Colin G, Chamaillard Y (2013) Optimal energy management strategy including battery health through thermal management for hybrid vehicles. IFAC Proc Vol 46(21):384–389

Park H (2013) A design of air flow configuration for cooling lithium ion battery in hybrid electric vehicles. J Power Sources 239:30–36

Park S, Jung D (2013) Battery cell arrangement and heat transfer fluid effects on the parasitic power consumption and the cell temperature distribution in a hybrid electric vehicle. J Power Sources 227:191–198

Perez RE, Liu HH, Behdinan K (2004) Evaluation of multidisciplinary optimization approaches for aircraft conceptual design. In: AIAA/ISSMO multidisciplinary analysis and optimization conference, Albany, NY

Ponchaut N, Colella F, Somandepalli V, Stern M (2014) Thermal management modeling for thermal runaway avoidance in lithium-ion batteries

Rao CR (1947) Factorial experiments derivable from combinatorial arrangements of arrays. Suppl J R Stat Soc 9(1):128–139

Rao Z, Wang S (2011) A review of power battery thermal energy management. Renew Sust Energ Rev 15(9):4554–4571

Sellar R, Batill S, Renaud J (1996) Response surface based, concurrent subspace optimization for multidisciplinary system design. AIAA Pap 714:1996

Severino B, Gana F, Palma-Behnke R, Estévez PA, Calderón-Muñoz WR, Orchard ME, Reyes J, Cortés M (2014) Multi-objective optimal design of lithium-ion battery packs based on evolutionary algorithms. J Power Sources 267:288–299

Smith J, Hinterberger M, Hable P, Koehler J (2014) Simulative method for determining the optimal operating conditions for a cooling plate for lithium-ion battery cell modules. J Power Sources 267:784–792

Sobieszczanski-Sobieski J, Agte JS, Sandusky RR (2000) Bilevel integrated system synthesis. AIAA J 38(1):164–172

Sobol' IM (1967) On the distribution of points in a cube and the approximate evaluation of integrals. Zhurnal Vychislitel'noi Matematiki i Matematicheskoi Fiziki 7(4):784–802

Somasundaram K, Birgersson E, Mujumdar AS (2012) Thermal–electrochemical model for passive thermal management of a spiral-wound lithium-ion battery. J Power Sources 203:84–96

Stein ML (2012) Interpolation of spatial data: some theory for kriging. Springer Science & Business Media

Sun H, Dixon R (2014) Development of cooling strategy for an air cooled lithium-ion battery pack. J Power Sources 272:404–414

Sun W, Wang X, Wang L, Zhang J, Song X (2016) Multidisciplinary design optimization of tunnel boring machine considering both structure and control parameters under complex geological conditions. Struct Multidiscip Optim, 1–20

Vapnik VN, Vapnik V (1998) Statistical learning theory, vol 1. Wiley, New York

Wang D, Coignard J, Zeng T, Zhang C, Saxena S (2016) Quantifying electric vehicle battery degradation from driving vs. vehicle-to-grid services. J Power Sources 332:193–203

Wang J, Purewal J, Liu P, Hicks-Garner J, Soukazian S, Sherman E, Sorenson A, Vu L, Tataria H, Verbrugge MW (2014) Degradation of lithium ion batteries employing graphite negatives and nickel–cobalt–manganese oxide+ spinel manganese oxide positives: Part 1, aging mechanisms and life estimation. J Power Sources 269:937–948

Ye Y, Saw LH, Shi Y, Tay AA (2015) Numerical analyses on optimizing a heat pipe thermal management system for lithium-ion batteries during fast charging. Appl Therm Eng 86:281–291

Zhang J, Chowdhury S, Zhang J, Messac A, Castillo L (2013) Adaptive hybrid surrogate modeling for complex systems. AIAA J 51(3):643–656